Minerals Engineering 211 (2024) 108679

Contents lists available at ScienceDirect

Minerals Engineering

journal homepage: www.elsevier.com/locate/mineng

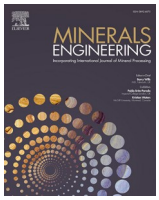

Electrochemical cobalt oxidation in chloride media

Iryna Makarava [a,*], Jere Vänskä [a], Agnieszka Kramek [b], Jacek Ryl [c], Benjamin P. Wilson [a], Kirsi Yliniemi [d], Mari Lundström [a,*]

[a] Department of Chemical and Metallurgical Engineering, School of Chemical Engineering, Aalto University, P.O. Box 16200, Vuorimiehentie 2, 02150 Espoo, Finland
[b] Faculty of Mechanics and Technology in Stalowa Wola, Rzeszow University of Technology, Kwiatkowskiego Str. 4 Stalowa Wola, PL-37450, Poland
[c] Institute of Nanotechnology and Materials Engineering, Faculty of Applied Physics and Mathematics, Gdansk University of Technology, Narutowicza Str. 11/12 Gdansk, PL-80233, Poland
[d] Department of Chemical and Materials Science, School of Chemical Engineering, Aalto University, P.O. Box 16100, Kemistintie 1, 02150 Espoo, Finland

ARTICLE INFO

Keywords:
Oxidation
Electrochemistry
Cobalt oxide
Cobalt hydroxide
Cobalt oxyhydroxide

ABSTRACT

The green transition, despite recent advances in cobalt-free battery technologies, is still highly dependent on the availability of critical cobalt-based materials. Consequently, there has been increasing interest towards the development of new methods that maximize critical metals recovery from industrial hydrometallurgical solutions. In the current study, direct anodic oxidation of cobalt species from cobalt chloride solutions was studied as one alternative future strategy for cobalt recovery. Electrochemical methods were used (cyclic voltammetry, potentiostatic anodic deposition) and the effect of pH, temperature, and the concentration of cobalt and chloride ions on cobalt precipitation were investigated. The increase of pH and temperature was shown to stabilize the electrochemical oxidation of cobalt, while a decrease in cobalt concentration had a negative effect on precipitation. Scanning Electron Microscope, Atomic Force Microscopy and X-ray Photoelectron Spectroscopy were exploited to evaluate the morphology, structure, and composition of obtained anodic product. Calculated for potentiostatic anodic deposition (at highest studied potential of 1300 mV vs. Ag/AgCl) nucleation mechanism shows that the rate of nucleation for oxygen-cobalt species is faster than the subsequent growth rate of nuclei (instantaneous mechanism). XPS results confirmed that mixed Co_3O_4/$Co(OH)_2$/CoOOH precipitate could be obtained by optimized anodic potentiostatic deposition in the range from 900 to 1150 mV and pH from 3 to 6 at 60 °C.

1. Introduction

Cobalt is a significant for technology metal used e.g., in aircraft engines, cemented carbides, lithium-ion batteries, superalloys, gas turbines, pigments, chemical catalysts, and permanent magnets (EU Commission, 2017; IEA, 2021; Rahimpour Golroudbary et. al., 2022). Cobalt has been identified as a critical material due to the scarcity of natural resources, and its high demand (Crundwell et al., 2011; Godoy León and Dewulf, 2020). For example, over the last decade alone the global requirement for cobalt has tripled and is further predicted to double again by 2035 (Calvão et al., 2021). More specifically, the current high demand for cobalt is related to the growth of electric vehicles and their related lithium-ion batteries that may require a total supply that exceeds the globally known reserves (W. Liu et al., 2023). Moreover, the cobalt supply chain is also subject to periods of volatility as nearly half of global cobalt mining is concentrated in the Democratic Republic of Congo (Gulley, 2022).

Cobalt and nickel have traditionally been recovered from sulfide and laterite ores by both pyrometallurgical and hydrometallurgical techniques (Crundwell et al., 2011). The raw materials are sulfide, oxide, and arsenide ores (Dehaine et al., 2021; Giebner et al., 2019) and the usual ratio between cobalt and nickel in ores is such that cobalt can be considered a byproduct (Giebner et al., 2019; Torjus, 2008). The hydrometallurgical refining route for cobalt usually includes leaching of ores (Zheng et al., 2023), neutralization to remove impurities such as Fe, Al, and Cr (Faris et al., 2021), and precipitation of a mixed Ni/Co intermediate, such as mixed hydroxide precipitate, mixed carbonate precipitate or mixed sulfide precipitate (Ichlas et al., 2020). Furthermore, such solids are often re-leached and subjected to solvent extraction for the further removal of impurities (such as manganese) and/or the separation of cobalt from nickel and manganese as high purity products (Astuti et al., 2023; Jantunen et al., 2022; Yuan et al., 2022). For the

* Corresponding authors.
E-mail addresses: Iryna.Makarava@aalto.fi (I. Makarava), Mari.Lundstrom@aalto.fi (M. Lundström).

https://doi.org/10.1016/j.mineng.2024.108679
Received 27 October 2023; Received in revised form 28 February 2024; Accepted 25 March 2024
Available online 5 April 2024

battery industry, cobalt is typically crystallized as cobalt sulphate salt in primary refining, and further processed to Li-Co-Ni-Mn oxides at pCAM and CAM production via hydroxide precipitation and high temperature calcination (Välikangas et al., 2020). However, also cobalt oxides can also be used in other applications such as ceramic industry (Metz et al., 2010). Therefore, the state-of-the-art metallurgical cobalt refining can be considered as a relatively complex and chemical-intensive processing route.

With the increasing demand for cobalt, and with a focus on energy and material efficiency in processing, alternative cobalt recovery routes are being studied. Electrochemical methods such as oxidative anodic precipitation could potentially provide alternative less chemical-intensive strategies for metal recovery, especially when used in conjunction with renewable energy sources. The process of electrooxidation of cobalt has been earlier studied in $CoCl_2$ (Das and Das, 2010; Z. Liu et al., 2005), $CoSO_4$ (Ivanova et al., 2003) or $Co(NO_3)_2$ (Heli and Yadegari, 2010; Zhou et al., 2009) solutions. Electrooxidation of cobalt from chloride solutions has been suggested having advantages, like high electrolyte conductivity, low electrolyte viscosity, low anodic and cathodic overpotentials, and higher activity of the cobalt ion, resulting in less sensitivity towards fluctuations in electrolyte pH (Åkre, 2008). However, chloride solutions are more corrosive than sulphate solutions and in chloride media chlorine evolution is kinetically favored, thus, advanced cell designs are needed for the safe handling of toxic chlorine that could be produced at the anodes (Åkre, 2008; G. Liu et al., 2016). For industrial production the formation of Cl_2 or O_2 at the anode can also be considered as advantage, when used oxidant in hydrometallurgical leaching operations (Anderson, 2014).

Pourbaix diagram of Co bulk phases built by HSC software at temperatures 60 °C, $c(Co^{2+}) = 55$ g/L, $c(Cl^-) = 65$ g/L without taking into account CoOOH, is represented in the Fig. 1S (Supplementary material).

In aqueous solutions, cobalt-ions predominantly exist as $CoCl^+$ or as Co^{2+} in acidic or neutral media (Bajdich et al., 2013). When the acidic media is introduced to high potentials (1.2 – 1.4 V vs. Ag/AgCl), Fig. S1, Co^{2+} ions are stable. However, at higher potentials and/or higher pHs cobalt can also form oxides such as Co_3O_4 or CoOOH. Oxide precipitation phenomena are not solely dependent on pH but are also electrochemical in nature, indicating that Co^{2+} needs to oxidize to precipitate as Co_3O_4. Black cobalt oxide is known as a selective coating material for high-temperature solar collectors and is superior to the generally used black chrome coatings, while CoOOH has been suggested as a promising material for fuel cells and capacitors (Kelpšaite et al., 2011). Zhang and co-workers (Zhang et al., 2012) have reported a strategy to grow Co_3O_4 by electrochemical oxidation. Firstly, $Co(OH)_2$ was obtained by electrochemical oxidation of the electrodeposited Co layer and further polycrystalline Co_3O_4 was formed by thermal treatment step. Another possibility to obtain Co_3O_4 (Karami and Chidar, 2015) or mixture of Co_3O_4/CoOOH (Chernysheva et al., 2018) electrochemically has been demonstrated via pulsed current anodic deposition from $Co(OH)_2$. Additionally, CoOOH can be selectively obtained by oxidation of crystalline $Co(OH)_2$ in alkaline media (IEA, 2021;Aguilera et al., 2020).

With further increase in potential, cobalt may also oxidize electrochemically into valence of 3+ and theoretically form CoOOH either directly from solution (at pH ~ 4–6) or via Co_3O_4 formation at higher pHs, (Kudielka et al., 2017). At the area of oxygen evolution, CoOOH has been reported being the most stable phase (Moysiadou et al., 2020; Yu et al., 2020).

Thermodynamically the precipitation of cobalt in any of the above mentioned forms of oxide/hydroxide/oxyhydroxide Co_3O_4/$Co(OH)_2$/CoOOH occurs preferentially at higher pHs (hydroxide) and/or at higher oxidative potentials and temperatures (oxides). At potentials 1 to 1.3 V vs Ag/AgCl and pH 4–6 there is a possibility to obtain CoOOH which was proved by Bajdich et al. (2013) that represented it in Pourbaix diagrams of Co ($C_{Co} = 10^{-6}$ mol kg^{-1}; 25 °C).

The previous scientific literature was dominantly focused on the creation of cobalt oxide films e.g. for the purposes of catalysis for CO (Kelpšaite et al., 2011) or water oxidation (Bajdich et al., 2013; Moysiadou et al., 2020; Zhang et al., 2012), thus previous research were focusing on dilute solutions that additionally contained additives, such as buffers. To the best of our knowledge, the electrooxidation of cobalt for further recovery from primary and secondary cobalt-containing hydrometallurgical streams has been overlooked in scientific literature. In the present work, we investigate the electrochemical oxidation behavior of cobalt in solutions mimicking industrial cobalt refinery solutions. With the aim of facilitating the electrification of metallurgy, there is a pressing need to construct prospective strategies for the direct electrochemical recovery of cobalt. Therefore, it can pave the way towards the integration of efficient and sustainable techniques in metallurgical processes.

2. Experimental

2.1. Materials

Cobalt chloride, $CoCl_2 \cdot 6H_2O$ (Thermo Scientific, 98 %), MilliQ water (Merck Millipore Q-POD) 0.1 M or 0.5 M NaOH (Sigma-Aldrich, ≥ 99.8 %), HCl (VWR Chemicals, 36.5 %) were used for solution preparation which mimics an industrial hydrometallurgical process solution (Agarwal et al., 2019). The solutions investigated had the composition presented in the Table 1.

2.2. Electrochemical measurements

Electrochemical measurements were carried out in a three-electrode cell with the volume of a solution of 100 mL with saturated silver/silver chloride as reference electrode (RE, SI Analytics, Germany), platinum (Kultakeskus Oy, Finland) as counter electrode – 8 cm^2 (CE) and working electrode – 1.6 cm^2 (WE) using an IviumStat 24-bit CompactStat potentiostat (Ivium Technologies, Netherlands). Platinum electrodes were prepared by etching in 35 % HCl, and finally degreasing with ethanol, thoroughly washing with DI water. The distance between the WE and CE was fixed at 2 cm. Prior to the experiments, working electrodes were immersed in the electrolyte for 30 min.

Cyclic voltammetry (CV) was undertaken in all *Solutions* (1–3) to study the electrochemical oxidation and reduction reactions of cobalt under at pHs 3–6. CVs were obtained to the anodic direction and back (0.5 – 1.2 – 0 – 1.5 V vs. Ag/AgCl) at a 25 mV/s scan rate (and 1, 5, 25, 50, and 100 mV/s scan rate for studying of scan rate dependence). Two cycles were recorded, and the second cycle was regarded as being representative for each measurement and negligible difference was found between the first and second scans. The temperature was controlled by a water-jacketed cell and a thermostat with all measurements performed at 60 ± 1 °C except for the temperature effect experiments which used a range from 20 to 60 °C.

Anodic deposition (potentiostatic experiments) was carried out at potentials 300, 500, 700, 900, 1150, and 1300 mV vs Ag/AgCl without stirring to observe cobalt oxide deposition at a defined potential. The initial stage (60 s) and long-term (2 h) electrooxidation were recorded to study the kinetics, and growth and to allow the deposition product to be characterized, respectively. The temperature used was 60 ± 1 °C in a 150 mL glass beaker and the solution compositions utilized are outlined in Table 1. The pH of the solution was monitored using a pH meter (Seven Excellence, Mettler Toledo), and the temperature of the electrolyte was controlled by a thermostatic water bath (Isotemp, Fisher

Table 1
Synthetic cobalt chloride solutions investigated.

Solution	Co (g/L)	Cl (g/L)	Na (g/L)	T (°C)	pH
Solution 1	55	65	–	20–60	1–6
Solution 2	5.5	6.5	–	60	3
Solution 3	55	72.5–100.5	2.3–23	60	3

Scientific, U.S.A.).

2.3. Characterization methods

Surface morphology and composition of all anodic deposits were measured using Mira^2 Tescan GM (Czech Republic) scanning electron microscopy (SEM) equipped with an energy dispersive X-ray (EDS, Thermo Fisher Scientific, U.S.A.) unit. The reported deposit chemical compositions (as atom percent) comprise of average EDS values from 10 point/area spectra.

Surface profiles of the anodic deposits obtained from the solutions of 55 g/L Co at pH 3 and pH 6 (*Solution 1*) were measured in air using atomic force microscope (AFM, MultiMode 8, Bruker, U.S.A.). The mapped area (10 × 10 μm) was scanned with Bruker SCM-PIT probe with spring constant of ~ 2.8 N/m, resonant frequency of ~ 75 kHz and tip radius of ~ 20 nm. The tip speed was 8 μm/s, image resolution 512 × 512 pixels, and tip lift height 50 nm. AFM data was analyzed using Nanoscope Analysis V1.15 software. The first order plane fit, and zeroth-order flattening were used to process the height maps.

Thermogravimetric analyses (TGA, Netzsch STA 449 F3 Jupiter & QMS 403 Aëolos Quadro, Germany) of anodic deposits obtained from the solutions of 55 g/L Co at pH 3 and pH 6 (*Solution 1*) were recorded and analyzed by the Netzsch Proteus software (version 6.1.0).

X-ray photoelectron spectroscopy (XPS, ThermoFisher Scientific, U.S.A.) was used for the characterization of cobalt precipitates produced after 2 h of potentiostatic anodic deposition (900 mV and 1150 mV vs. Ag/AgCl). Prior to analysis, samples were cleaned in deionized water for 10 min and dried with no other treatment implemented in order not to compromise the subtle chemical changes on the surface. Spectra were recorded in the Co2p, Cl2p, C1s and O1s binding energy (BE) range for each sample to verify their surface chemistry. The measurements were carried out using XPS K-Alpha (ThermoFisher Scientific, U.S.A.) equipped with a monochromated small-spot of X-ray source (diameter of 0.65 mm). Applied pass energy was 10 eV and the energy step size 0.1 eV. Charge compensation was controlled through low-energy electron and low-energy Ar^+ ions emission using a flood gun (emission current 0.15 mA) which provided an XPS analysis depth of approximately 5 nm. Data were analyzed with software Avantage version 5.975.

3. Results and discussion

3.1. Oxidation and reduction reactions in cobalt(II) chloride solutions

Effect of the solution pH and temperature on the electrochemical behavior of cobalt.

Cyclic voltammetry (in *Solution 1*) showed that there were negligible oxidation peaks detectable in the voltammograms - up to 0.15 mA/cm^2 – while in the potential range from 0.9 to 1.15 V vs. Ag/AgCl some peaks can be observed and a more substantial and rapid current increase is clearly evident at potentials higher than 1.15 V vs. Ag/AgCl, Fig. 1. The oxidation behavior of cobalt was found to be slightly different at all investigated pHs (3–6). In particular, at pH 3 an oxidation peak a_{p1} was observed in the region 0.4–0.7 V vs. Ag/AgCl, while at pH 5 and at pH 6 there is a clear oxidation (peak a_{p2}) reaction, initiating in the region from 0.6 to 1.1–1.2 V vs. Ag/AgCl. There is also a clear tendency for the size of the reduction peak c_{p1} to increase (during the reverse sweep) with the change in pH from 3 to 6 and this is consistent with previous polarization behavior measured by (Pontinha et al., 2006; Vittal & Ho, 2015). Such an increase of reduction peak has been suggested as being related to different cobalt oxide species and their relevant allotropic phases, which furthermore can be strongly influenced by hydration effects (Vittal and Ho, 2015).

The region of anodic peak a_{p1} in the Fig. 1 at 0.9 V vs. Ag/AgCl is expected to be associated with $Co_3O_4/Co(OH)_2$ film formation by Eq. (1) and (2) (Vittal and Ho, 2015):

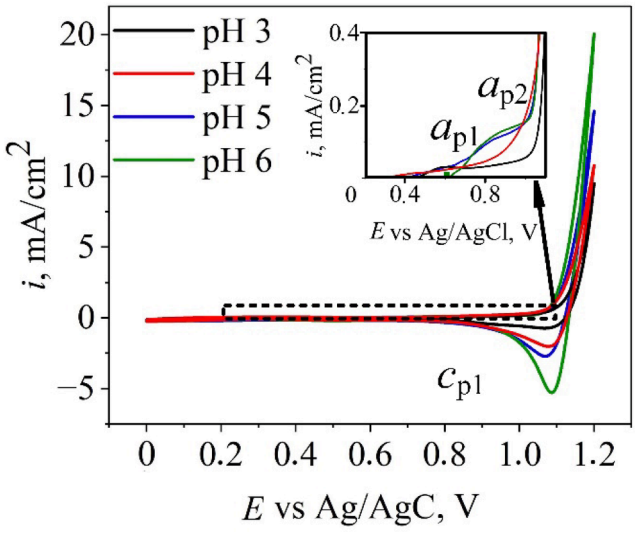

Fig. 1. Cyclic voltammograms recorded at a Pt electrode in *Solution 1* at a temperature 60 °C scan rate of 25 mV·s^{-1}; Insert part is marked in rectangle area of CV. a_{p1}, a_{p2} and c_{p1} refers to the anodic and cathodic peaks observed.

$$3CoCl^+_{(aq)} + 8OH^-_{(aq)} \rightarrow Co_3O_{4(s)} + 4H_2O_{(aq)} + 3Cl^-_{(aq)} + 2e^- \quad (1)$$

$$CoCl^+_{(aq)} + 2OH^-_{(aq)} \rightarrow Co(OH)_{2(s)} + 2Cl^-_{(aq)} + e^- \quad (2)$$

At the high oxidation potential > 1.15 V vs. Ag/AgCl a significant increase in the recorded anodic current was observed that may correspond to the oxidation of $CoCl^+/Co(OH)_2$ or Co_3O_4 into CoOOH (Lisnund et al., 2022), as indicated by Eq. (3)–(5):

$$CoCl^+_{(aq)} + 2OH^-_{(aq)} \leftrightarrow CoOOH_{(s)} + 2H_2O_{(aq)} + e– \quad (3)$$

$$Co(OH)_{2(s)} + OH^-_{(aq)} \leftrightarrow CoOOH_{(s)} + 2H_2O_{(aq)} + e– \quad (4)$$

$$Co_3O_{4(s)} + H_2O_{(aq)} + OH^-_{(aq)} \leftrightarrow 3CoOOH_{(s)} + e– \quad (5)$$

The reduction peak C_{p1} measured at 1.1 V vs. Ag/AgCl may be related to the conversion of CoOOH into $CoCl^+/Co(OH)_2$ (a reverse of the reactions in Eq. ((3)–(5)). As a result, the electrodeposited CoO_x in this potential region may theoretically consist of different cobalt-containing phases, including Co_3O_4, $Co(OH)_2$, and CoOOH.

A more detailed analysis (Fig. 2, *Solution 1*) shows that cobalt oxidation reactions occur in the range between 0.3 V and 1.15 V vs. Ag/AgCl (Fig. 2) and that the increase in temperature (20 to 60 °C) leads to changes in the anodic and cathodic current densities at both pH 3 and 6. It has been reported that high temperature is beneficial through higher local pH that favors the anodic deposition of cobalt (Åkre, 2008); besides, it is known that high temperature promotes Cl_2 selectivity versus O_2 (Hägg, 2000; Spasojević et al., 2012; Vos et al., 2019). The increase in solution pH slightly decreases the size of the first oxidation peak (a_{p1} at E ~ 0.6 V vs. Ag/AgCl), while the second anodic peak (a_{p2}) clearly increases. Both observations correlate with the phenomena previously discussed in relation to Fig. 1. Interestingly, the anodic current is very similar for temperatures 50 and 60 °C at pH 6, Fig. 2b, which may be connected to the mass-transfer controlled reaction of cobalt oxide deposition (Åkre, 2008), competing dissolution reactions or possible even to a surface passivation. These results indicate that the stability of the oxide/oxyhydroxide layer (Koga et al., 2009), which can be predicted as the major cobalt product within this potential range, is increased with higher temperatures.

3.1.1. Effect of chloride ions on the electrochemical behavior of cobalt.

The electrochemical behavior of cobalt was further studied with *Solution 3* that contained 55 g/L Co^{2+} (Table 1) in the presence of

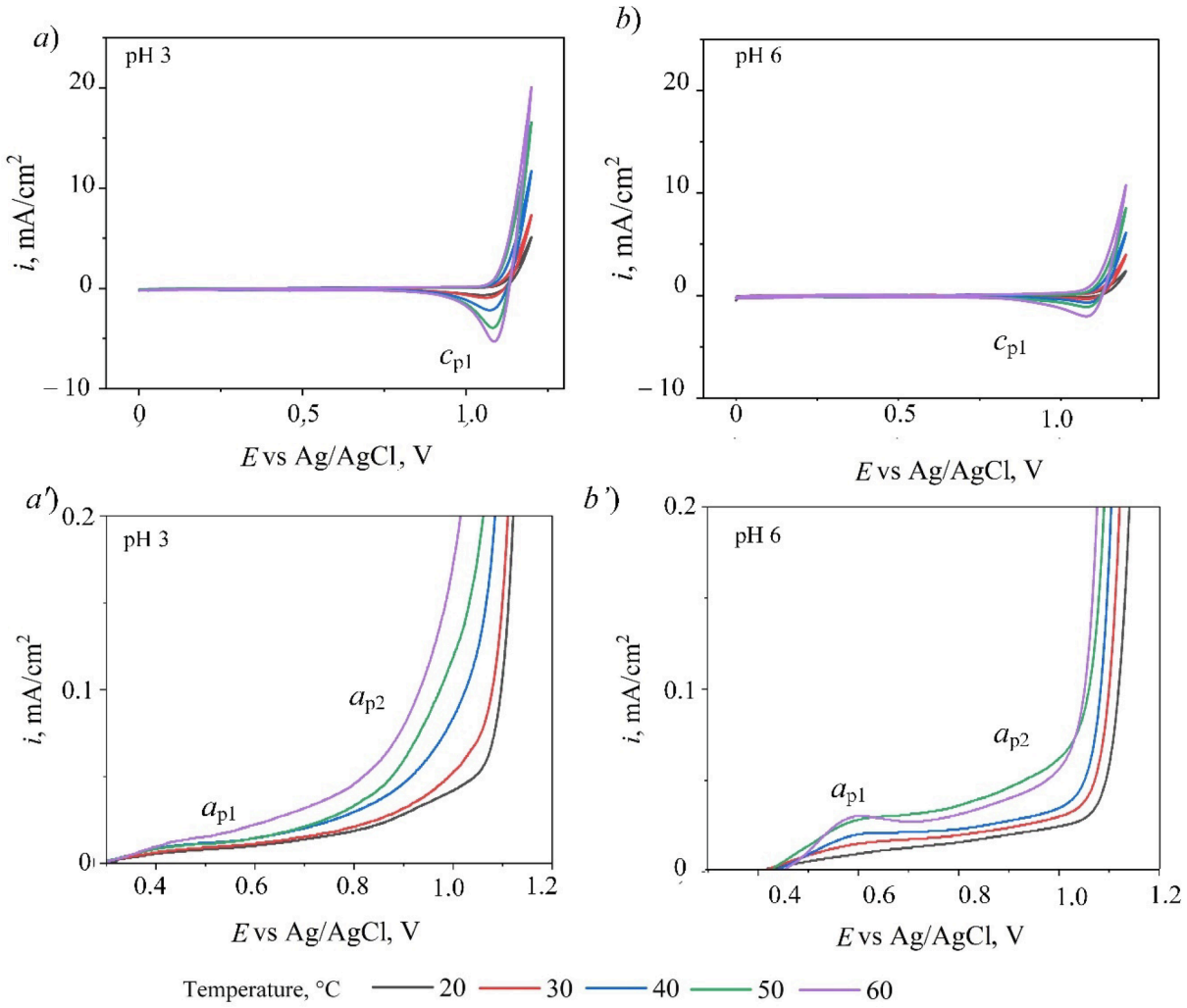

Fig. 2. (*a*, *b*) Cyclic voltammetry at pH 3 and pH 6 at a scan rate of 25 mV·s^{-1} with 55 g/L Co^{2+}(*Solution 1*) and (*a'*, *b'*) magnified range of potentials of 0.3 to 1.2 V vs. Ag/AgCl and T = 20 – 60 °C.

additional chloride ions at $T = 60$ °C, Fig. 3.

Generally, the oxidation behavior of cobalt was found to be similar in both absence (Fig. 2) and presence of additional chlorides (NaCl), Fig. 3., as two oxidation peaks are clearly visible at 0.5 V and around 0.9 V vs. Ag/AgCl, Fig. 3b. Addition of chloride (NaCl until 1 M) increased the current density of both cobalt oxidation peaks a_{p1} and a_{p2} (Fig. 3b)

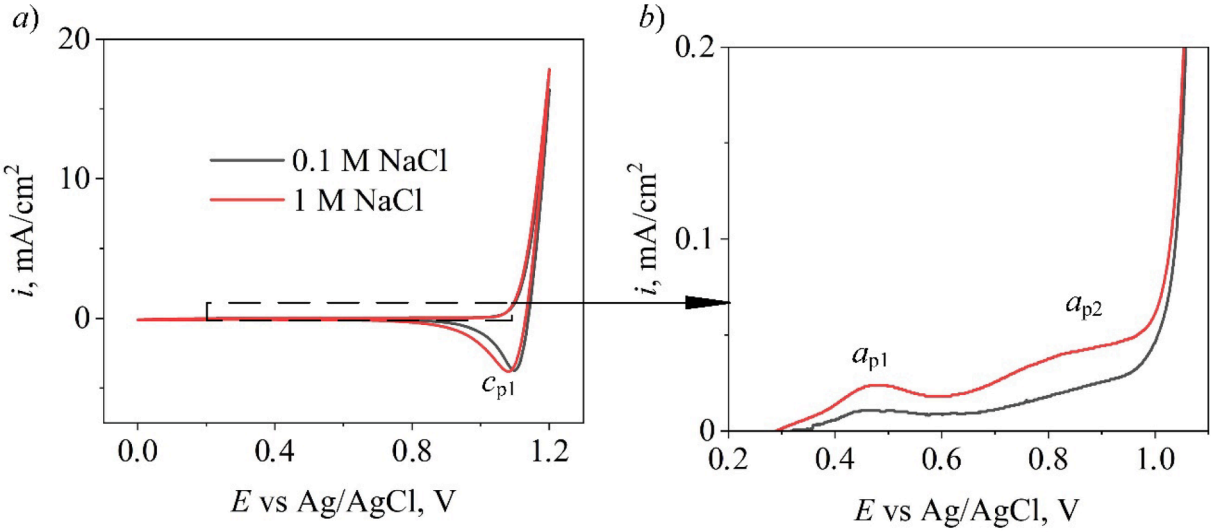

Fig. 3. (*a*) Cyclic voltammetry in *Solution 3* at a scan rate of 25 mV·s^{-1} at $T = 60$ °C and (b) magnified anodic area marked as a rectangle.

compare to 0.1 M NaCl, which indicates that the presence of Cl^- enhances the oxidation reactions of cobalt. Moreover, an increasing Cl^- concentration (NaCl) in the process solution was also shown to lead to an electronegative shift of the reduction peak (c_{p1}), Fig. 3a, between 1.15 and 0.8 V vs. Ag/AgCl (Fig. 3a). A significant increase of chloride-ions might lead to predominant chlorine evolution because the generation of O_2 is less reversible (Vos et al., 2019).

3.1.2. The effect of time on cobalt oxidation at constant potentials.

Potentiostatic experiments at pre-defined potentials (Fig. 4 and Fig. 5) were conducted to better determine the oxidation mechanisms involved in the formation of the anodic deposits at different pHs, and cobalt concentrations. The results show that at potentials from 300 to 900 mV vs. Ag/AgCl, only small steady currents were obtained in *Solution 1* (Fig. 4, *a–c*) regardless of the solution pH. At 900 mV some oxidative reactions (Eq. (1), (2)) may already occur, depending on the pH of the solution. At pH 3 some current density is observed during the initial 15 sec (Fig. 4b,c), and after that current is equal to zero which can be connected to the passivation of the surface, particularly, with differences in crystallographic forms of oxides that appear at the electrode. However, at higher pH 6 there is a decay of current during the first 15 sec, after that the current density i.e. the oxidative reactions remains stable during 2 h (as shown in Fig. S3, *a'–c'*).

At potential 1150 mV higher pHs 2–6 can clearly initiate oxidation

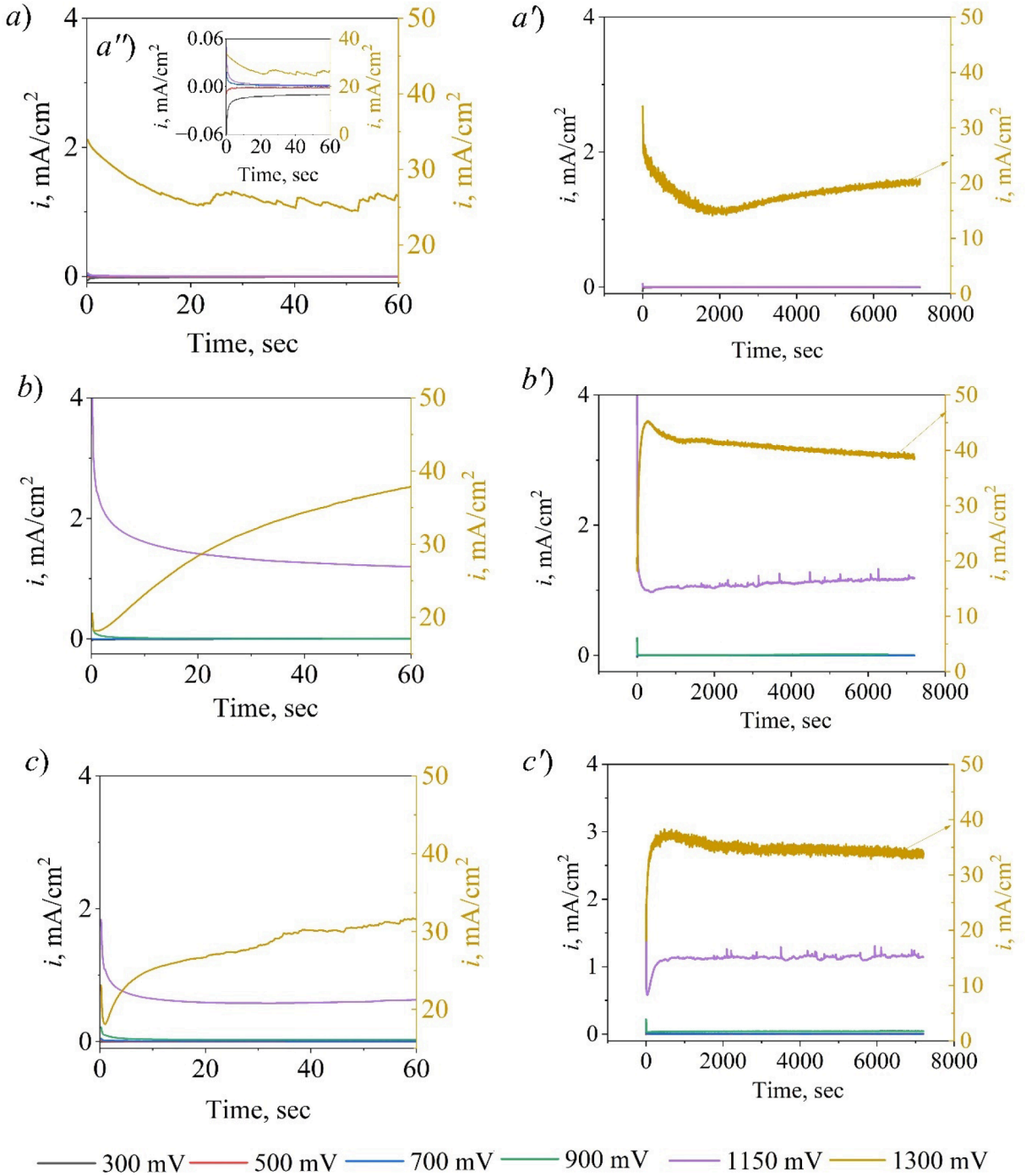

Fig. 4. Potentiostatic cobalt deposition in *Solution 1* at $T = 60$ °C at different potentials and (*a*, *a'*) pH 1, (*b*, *b'*) pH 3, (*c*, *c'*) pH 6 where *a–c* is 60 sec, *a'–c'* – 7200 sec; Insert part in Fig *a* - (*a''*) is enlarged area by y-axis. Separate y-axis includes only 1300 mV vs. Ag/AgCl due to larger currents.

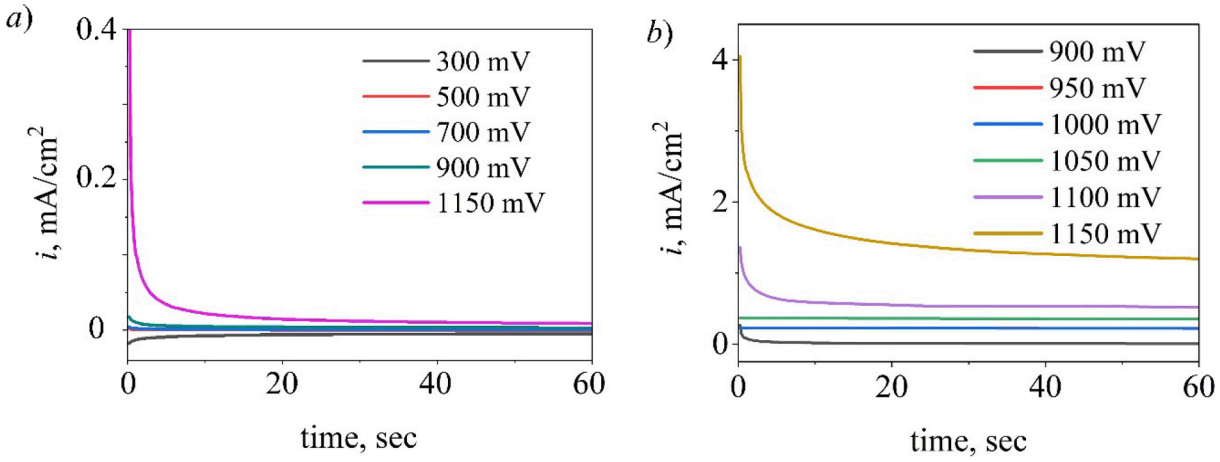

Fig. 5. (*a*) Potentiostatic anodic deposition in *Solution 2* at pH 3 and $T = 60$ °C; (*b*) Potentiostatic anodic deposition in *Solution 1* at T = 60 °C at pH 3 and range of potentials from 900 mV to 1150 mV.

reactions (Fig. S3a), whereas the lowest pH (pH 1) could initiate very little oxidation reactions can be observed, These curves are shown to have two features at the initial step of the curve, the decay of current during the time as the reaction is controlled by the diffusion of active ions and the electroactive species around the electrode are consumed rapidly over time (Fig. 4b,c) followed by a rapid rise of current density. Current, finally, became stable for 1150 mV vs. Ag/AgCl after 15 min, Fig. 4b',*c'*.

The decline of current density observed at 1300 mV vs. Ag/AgCl, *Solution 1* which corresponds to the charge of the electric double layer on the electrode surface (Fig. 4b,c), after that the current density gradually increased and reached the maximum value, which corresponds to a typical crystal nucleation/growth process (Zhou et al., 2018). An oxidation peak of current was found at 270 sec for pH 3 and 480 sec for pH 6 (Fig. 4c'). In these cases, after a current peak maximum is reached at 15 min, a slight decrease—which is pH dependent—is then observed during the following 2 h of anodic deposition due to the consumptions of cobalt ions at the electrode/solution interface. In contrast, at a potential = 1300 mV vs. Ag/AgCl, (Fig. 4a') in the pH 1 solution intensive chlorine/oxygen evolution occurs that resulted in the measured current instability.

The final pH after 2 h of anodic deposition in *Solution 1* at 700 and 900 mV vs. Ag/AgCl slightly decreased (Supplementary material, Fig. S2), while at 1150 mV and 1300 mV the drop was greater most likely due to higher levels of OH^- consumption during precipitation (Eq. (1)–(5)) and/or enhanced oxygen gas formation levels that generate H^+ ions (Eq.6):

$$H_2O \rightarrow O_2 + 4H^+ + 4e^- \quad (6)$$

The total charge calculated from potentiostatic anodic deposition was varied between 10^{-9} to 10^{-4} A·h in the range of potentials from 300 to 900 mV vs. Ag/AgCl, and increased to 10^{-3}–10^{-1} A·h at potentials 1150 and 1300 mV vs. Ag/AgCl.

A tenfold decrease of cobalt concentration, 5.5 g/L Co^{2+}, *Solution 2* (Fig. S5a, Supplementary material) was shown to lead to a significant decrease in the corresponding cobalt oxidation reactions (i.e. current densities) over the potential range from 300 to 1150 mV vs. Ag/AgCl. Moreover, after 2 h of anodic potentiostatic deposition the solution was found to have remained at pH 3 suggesting the absence of any reactions that involve oxygen evolution. More detailed analysis of the oxidation process between 900 and 1150 mV vs. Ag/AgCl with a step of 50 mV, Fig. 5b, revealed that the most intensive oxidation process occurred at 1000 and 1150 mV as the highest current density was observed.

3.2. Nucleation and growth of cobalt oxide

Current recorded during the transition from a no-reaction state to a steady reaction state can be used as an indicator of the type of nucleation mechanisms that take place. A Scharifker-Hills (SH) model was used to investigate the nucleation mechanism as the impact of different parameters can be effectively canceled out by normalizing i and t to the peak current i_m and peak time t_m, respectively. Instantaneous nucleation corresponds to a slow simultaeous growth of nuclei at a small number of active sites, whereas in contrast, progressive nucleation relates to the fast growth of nuclei on many active sites, all activated during the course of electrooxidation/reduction (Grujicic and Pesic, 2005). In order to distinguish between these two distinct mechanisms, chronoamperometric data are plotted using time–current coordinates. From a theoretical point of view, the current–time transients corresponding to instantaneous nucleation and progressive nucleation can be described by the following simplified relationships (Kasach et al., 2020).

$$(i/i_m)^2 = 1.9542(t/t_m)^{-1}\{1-\exp[-1.2564(t/t_m)]\}^2 \quad (7)$$

$$(i/i_m)^2 = 1.2254(t/t_m)^{-1}\{1-\exp[-2.3367(t/t_m)^2]\}^2 \quad (8)$$

Potentiostatic anodic deposition at 1150 mV vs Ag/AgCl shows a current maximum at an initial time of 0.2 sec and therefore were not examined. A comparison of the theoretical current–time curves of 1300 mV vs Ag/AgCl at both pH 3 and at pH 6 with the equivalent experimental measurements is presented in Fig. 6. The results indicate that the initial kinetics of cobalt oxidation on Pt substrate is governed by the three-dimensional instantaneous growth-nucleation mechanism. This is in contrast to the previous research of Surendranath et al. (2012) who found that in dilute cobalt solution (0.4 mM Co^{2+}) coating growth preferably took place by the progressive mechanism.

Calculated parameters for current transients at different pH and potential 1300 mV vs. Ag/AgCl are listed in Table 2. The results show that with increasing pH, the nucleation rate (N_0) of cobalt oxide decreased and are inline with data previously reported in the literature for the oxidation of similar system (Jung and Jun, 2016; Scheck et al., 2016).

$$N_0 = 0.065(1/(8\pi C V_m))^{1/2}(zFC/(i_m t_m))^2 \quad (9)$$

where C is the concentration of cobalt in the bulk solution, N_0 is the number density of active sites, zF is the molar charge transferred during anodic deposition, V_m is the molar volume of the deposited cobalt oxide.

Morphology of the cobalt precipitates obtained at Pt substrate under different potentials and pH obtained after 2 h of anodic potentiostatic

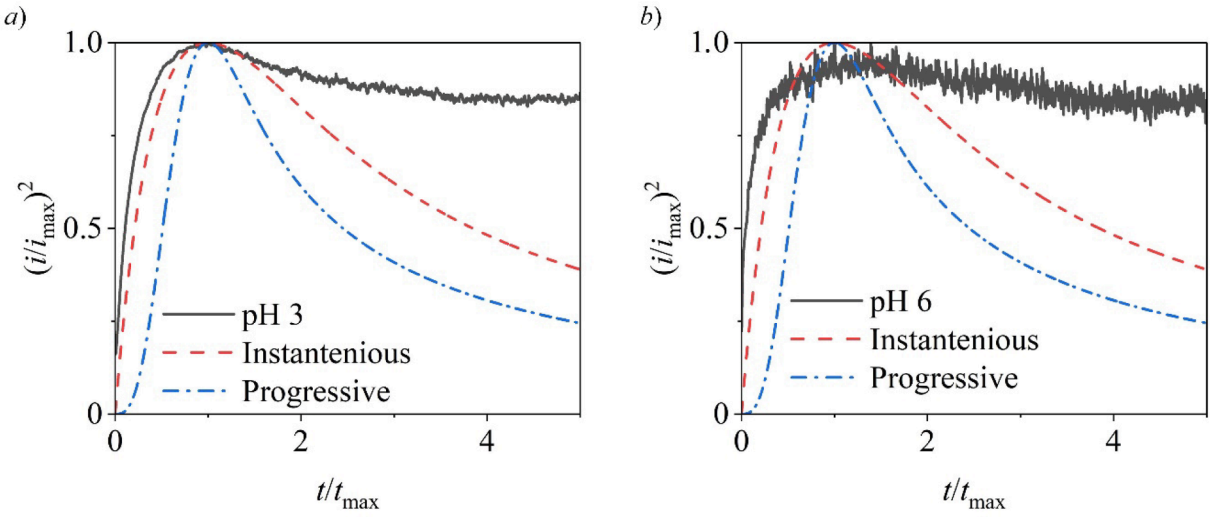

Fig. 6. Comparison of the dimensionless experimental current–time transients (applied potential is 1300 mV vs Ag/AgCl) for the electrooxidation of cobalt on Pt electrode with the theoretical transients for instantaneous and progressive nucleation at (*a*) pH 3, (*b*) pH 6.

Table 2
Nucleation parameters obtained from *Solution 1* at 1300 mV vs. Ag/AgCl.

pH	t_m, s	i_m, A/cm^2	$N_0.10^{-6}$, cm^{-2}
3	283 ± 0.06	0.045 ± 0.002	0.62 ± 0.12
6	476 ± 0.62	0.038 ± 0.005	0.44 ± 0.08

deposition are presented in Fig. 7. The surface morphology revealed an even distribution of film at potentials 1150 mV and 1300 mV, as after 2 h the surface is fully covered with precipitate. At lower pH (2 and 3) and low potentials, the Pt substrate is covered in discernible individual spherical grains that are agglomerated together in bigger clusters and similar structures, with a size around 5 μm, are found for all precipitates deposited at 1150 mV (Fig. 7a,c,f,*h*,*k*). A common feature for all the coated surfaces obtained is the presence of cracks associated with internal stresses. Generally, the morphology of precipitates obtained at 1150 mV is not strongly dependent on the pH range. Upon closer examination in Fig. 7c', it is evident that AFM analysis did not reveal any visible surface cracking. It is important to note, however, that the scanned area was limited to only 10 μm^2, potentially rendering it insufficiently comprehensive for a definitive conclusion of internal surface stresses. The surfaces according to AFM analysis were homogeneously covered and are relatively flat with an average roughness (R_a) measured for 10 μm × 10 μm area of 44.4 nm.

The composition of the precipitate obtained at 1150 mV vs. Ag/AgCl was examined by EDS analysis and the results are outlined in Table 3.

EDS analysis shows that a change in pH from 2 to 6 increases the amount of oxygen in the cobalt precipitate from 62.9 to 81.8 at%, which suggests the presence of higher cobalt oxidation states (Bajdich et al., 2013) and similar results have also found by Kouidri et al. (Kouidri et al., 2019) with increased substrate temperatures. The stoichiometric ratio between cobalt and oxygen can be seen to increase from 1:2 to 1:4 due to the change in pH from 2 to 6 and this observation can be attributed to the increasing of possibility of adsorption of oxygen and oxygen-contained species to the Co sites (Bajdich et al., 2013). Traces of chloride were observed due to the attachment of $CoCl_2$ to the surface of the anodic deposit. The presence of CoOOH was identified in the sample (1150 mV, pH 3 and pH6) by XRD analysis, Fig. S4a, however, it does not solely explain the Co:O ratio indicated by Table 3. Compared with the precipitate obtained at pH 3, the diffraction peak width of the precipitate at pH 6 was slightly narrower, indicating that increasing pH leads to a decrease in the size of grains, thereby illustrating that pH can also affect the morphology size.

To characterize the composition of the cobalt precipitates in more detail, the samples obtained from *Solution 1* at pH 3 and pH 6 (E = 1150 mV and 900 mV) were investigated by high-resolution X-ray photoelectron spectroscopy (XPS). The raw spectra were deconvoluted into their main components and the results are displayed in Fig. 8. and Fig. S2 (Supplementary material) Co 2p spectrum for both precipitates (900 mV and 1150 mV) consist of two main broad peaks corresponding to $2p_{1/2}$ and $2p_{3/2}$ spin–orbit lines along with two shakeup satellite peaks at 779.9 eV and 780.9 eV. The binding energies (BEs) of Co $2p_{1/2}$ and $2p_{3/2}$ are separated by 15 eV indicating the presence of Co^{3+} species on the surface. However, the ratios of Co^{2+}/Co^{3+} for all applied potentials and pH are three times higher than that expected for Co_3O_4, further indicating the presence of CoOOH species as previously suggested by Urgunde et al (2019). It is worth noting that Co^{2+} and high spin Co^{3+} contain unpaired d-electrons and therefore the resultant spectra of these metal cations possess a complex structure with broad combinations of overlapping features, therefore render deconvolution of cobalt compounds and identification of single preferably formed compound were challenging (Biesinger et al., 2009, 2011).

The O 1 s spectrum of the precipitates has a peak at 531.3 eV which is associated with the hydroxide group (OH^-) and three more peaks at 529.3, 531.5, and 532.3 eV that correspond to Co-O, oxygen vacancies and the presence of structural water (Fig. 8,*b*).

The morphology of the powder obtained during anodic potentiostatic deposition (1150 mV) after mechanical removal from the anode was studied by SEM (see Fig. S5). Sediment obtained from the solution with pH 3 has the form of small particles (powder with saturated black color), whereas an increase in pH up to 6 led to the formation of a well-organized precipitated film (black color similar to graphite) with visually good attachment to the Pt substrate. To study the decomposition process of the cobalt oxide prepared at different pH, TGA analysis was performed. As can be seen from the TGA curves in Fig. S5, the mass loss (~2 wt%) below 100 °C is caused by the loss of adsorbed water from the sample (Grujicic & Pesic, 2005). There is one rapid mass loss at 300 °C that is most probably due to the thermal decomposition of $Co(OH)_2$ into Co_3O_4 (Li et al., 2018). TGA analysis shows a similar composition of powder for both pH 3 and pH 6.

4. Discussion

The results of the current study indicate that anodic cobalt recovery can be conducted directly from solution (*Solution 1* and *Solution 3*, *[Co]* = 55 g/L) similar to that used at hydrometallurgical production plants.

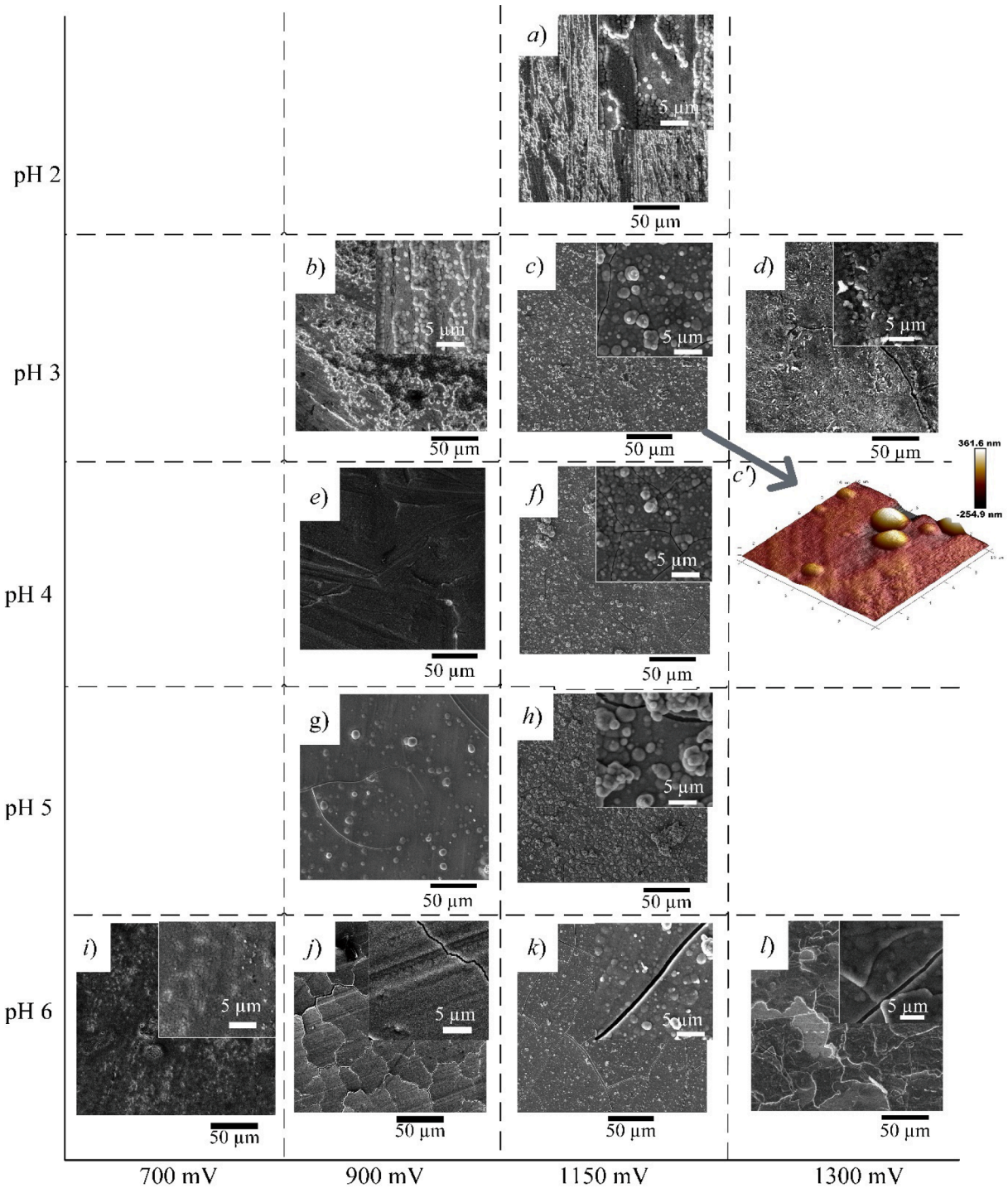

Fig. 7. (*a–f*) SEM of cobalt precipitate in 55 g/L Co^{2+} solution $T = 60$ °C at different potentials and pH; (*c'*) AFM of cobalt precipitate in at 1150 mV, pH 3.

Table 3
Elemental composition of film obtained by anodic potentiostatic deposition at 1150 mV vs. Ag/AgCl (EDS analysis).

at.%	pH 2	pH 3	pH 4	pH 5	pH 6
O	62.9	63.5	72.0	78.8	81.8
Cl	2.2	2.1	0.6	0.5	0.4
Co	34.9	34.4	27.5	20.7	17.8

Black color precipitate could be obtained anodically at conditions where pH was from 3 to 6 and potential ≥ 900 mV vs. Ag/AgCl. At lower potentials, no visible precipitate could be obtained, while lower pHs made the precipitate more oxygen deficient. In the precipitate, the intricate mixture encompasses a combination of Co_3O_4, α-$Co(OH)_2$, and γ-CoOOH, making it challenging to discern a single preferably formed compound. The results suggest also that high concentrations of cobalt (~55 g/L) are beneficial for anodic cobalt recovery, while competing reactions such as O_2 evolution may start to dominate in more dilute solutions (*Solution 2*).

The adhesion characteristics, observed visually, of the anodic

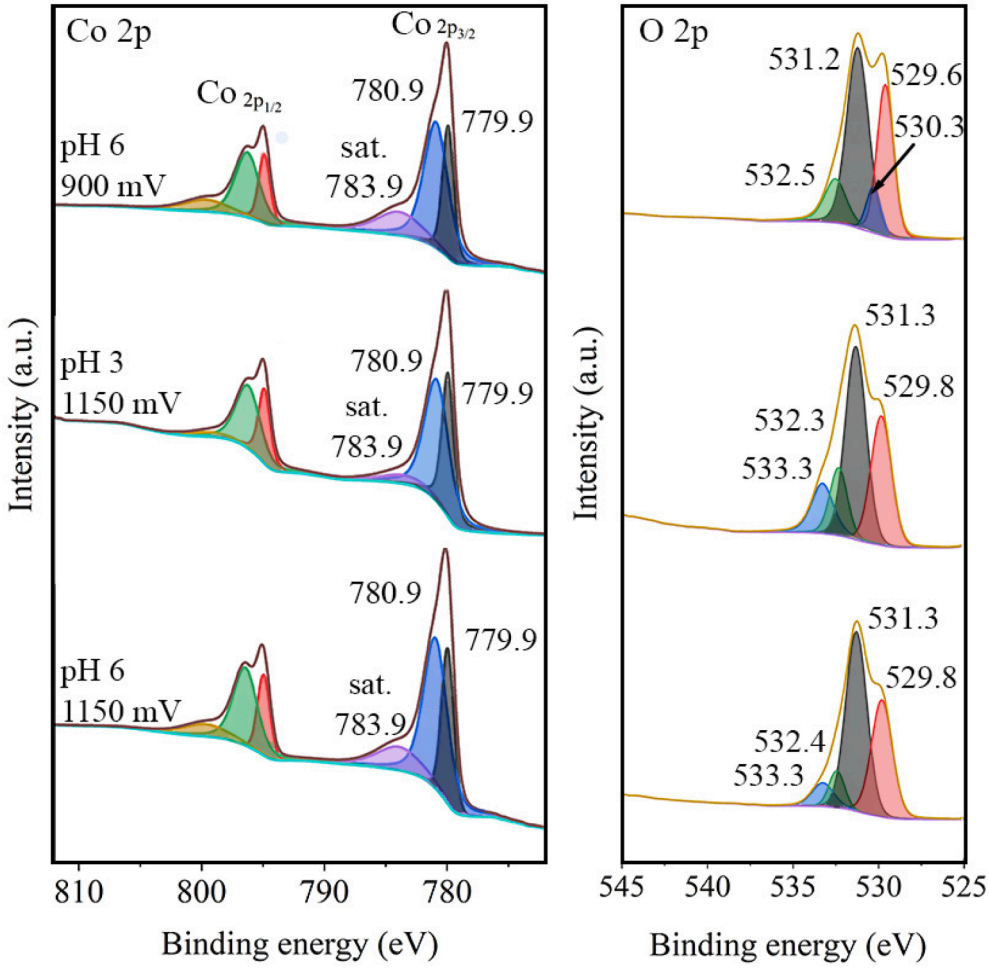

Fig. 8. High-resolution XPS spectra of (*a*) Co 2p and (*b*) O 2p for cobalt precipitate obtained at 1150 mV and 900 mV.

precipitate to the anodic surface are influenced by the pH of the solution and the concentration of Co^{2+}. An increase in pH and Co^{2+} concentration enhances the attachment of the precipitate to the surface. On the contrary, in more acidic solutions, the precipitates appear in a powdered form. Therefore, it is advisable to employ anode bags during anodic operation to collect particles from the slime. To our understanding, the pH of a solution impacts the chemical equilibrium between different cobalt species present in the solution as well as the precipitate particles. An increase in pH leads to changes in the speciation of cobalt ions in solution, affecting the nature and properties of the resulting cobalt oxide precipitate and, consequently, influence factors such as particle size and surface charge, all of which can influence adhesion to a substrate. Tombach (2009) showed that the specific adsorption of H^+/OH^- on surface hydroxyl groups, i.e., protonation and deprotonation reactions might result in pH-dependent charges on the surface of metal oxides. A similar finding was discovered in our previous work (Makarova et al., 2020) and was explained by the electrostatic attraction of particles to the electrode surface. On the other hand, the increase of pH may decrease the internal stresses of oxygen-contained film of cobalt on the Pt substrate.

While real industrial solutions can be highly pure after solution purification (solvent extraction of cobalt into the cobalt-rich phase), in the earlier stages of processing they also typically contain a variety of impurities (Harvey et al., 2011). The impact of impurities as well as processing efficiency and recovery were not studied in the current work, and need further to be addressed in order to make the evaluation of scalability or industrial applicability. Nevertheless, direct recovery and deposition of cobalt as a mixture of Co_3O_4, α-$Co(OH)_2$ and γ-CoOOH – or in the future even direct deposition of catalyzing cobalt-oxygen species surfaces from process solutions – is technically feasible and is a promising technology worthy of further investigation.

Solution pH and concentration of Co^{2+} influence the properties of the precipitate to attach to the anodic surface. Increasing of pH and Co^{2+} concentration increases attachment to the surface while raising solution acidity leads to powder type preicipitates that can be suggested as anode bags via anodic operation and collection of particles from the slime.

5. Conclusions

Electrochemical cobalt oxidation was studied in cobalt chloride solution by anodic potentiostatic deposition, and a mixed oxygen-based cobalt precipitate was grown on a Pt substrate surface. Cyclic voltammetry based on indicative Pourbaix diagram calculations showed that the increase of pH, the concentration of cobalt, and temperature has a positive effect on the oxidation process. Morphology of anodic cobalt precipitate produced at 1150 mV vs. Ag/AgCl were all found to be relatively flat with cracks and did show any noticable pH dependance. Potentiostatic anodic deposition based calculations indicated that the parameters of nucleation most likely involve the instantaneous growth of oxide film at 1300 mV vs. Ag/AgCl that usually results in the uniform size particles observed on the electrode surface rather than a progressive mechanism (Tan et al., 2021). Results from XPS confirmed the presence of three forms of cobalt, Co_3O_4, α-$Co(OH)_2$ and γ-CoOOH.

Overall, these results suggest a simple route to recover cobalt as Co-containing deposits. If successful, cobalt oxidation can be potentially used for direct recovery of cobalt from primary and secondary raw

material sources i.e. from hydrometallurgical solutions as an alternative and electrified recovery method. The method may in the future even be investigated as an direct formation functional material for application in energy storage devices.

CRediT authorship contribution statement

Iryna Makarava: Data curation, Formal analysis, Investigation, Methodology, Visualization, Writing – original draft, Writing – review & editing, Conceptualization, Validation. **Jere Vänskä:** Formal analysis, Investigation. **Agnieszka Kramek:** Investigation. **Jacek Ryl:** Investigation, Writing – review & editing. **Benjamin P. Wilson:** Writing – original draft, Writing – review & editing. **Kirsi Yliniemi:** Supervision, Conceptualization, Writing – original draft, Writing – review & editing. **Mari Lundström:** Conceptualization, Funding acquisition, Project administration, Resources, Supervision, Writing – original draft, Writing – review & editing.

Declaration of competing interest

The authors declare that they have no known competing financial interests or personal relationships that could have appeared to influence the work reported in this paper.

Data availability

No data was used for the research described in the article.

Acknowledgments

This work was supported by the European Union's Framework Programme for Research and Innovation Horizon Europe [Grant number: 101058124 (ENICON)]. The research also made use of the RawMatTERS Finland Infrastructure (RAMI) funded by the Academy of Finland and based at Aalto University, Espoo, Finland. Oluf Bøckman from Nikkelverk is acknowledged for information and discussions related to industrial nickel production solutions.

Appendix A. Supplementary data

Supplementary data to this article can be found online at https://doi.org/10.1016/j.mineng.2024.108679.

References

Agarwal V., Oksanen E., Wilson S., Aromaa, Bøckman J., Lundström O., 2019. Hydrothermal precipitation of nickel and cobalt oxides. In: Proceedings of the European Metallurgical Conference EMC, June 2019, vol. 2, Düsseldorf, Germany, pp. 793-805.

Aguilera, L., Aguiar, P.C.M., Ruiz, Y.L., Almeida, A., Moreira, J.A., Passos, R.R., et al., 2020. Electrochemical synthesis of γ-CoOOH films from α-$Co(OH)_2$ with a high electrochemical performance for energy storage device applications. J. Mater. Sci. Mater. Electron. 31, 3084–3091. https://doi.org/10.1007/s10854-019-02853-1.

Åkre, T., 2008. Electrowinning of cobalt from chloride solutions: anodic deposition of cobalt oxide on DSA. Norwegian University of Science and Technology.

Anderson, C.G., 2014. Innovations in nickel and cobalt Hydrometallurgy. Mineral Processing and Extractive Metallurgy 100, 403–426.

Astuti W, Nurjaman F, Rofiek Mufakhir F, Sumardi S, Avista D, Cleary Wanta K, et al. A novel method: Nickel and cobalt extraction from citric acid leaching solution of nickel laterite ores using oxalate precipitation. Miner Eng 2023;191. DOI: 10.1016/j.mineng.2022.107982.

Bajdich, M., García-Mota, M., Vojvodic, A., Nørskov, J.K., Bell, A.T., 2013. Theoretical investigation of the activity of cobalt oxides for the electrochemical oxidation of water. J Am Chem Soc 135, 13521–13530. https://doi.org/10.1021/ja405997s.

Biesinger, M.C., Payne, B.P., Lau, L.W.M., Gerson, A., Smart, R.S.C., 2009. X-ray photoelectron spectroscopic chemical state quantification of mixed nickel metal, oxide and hydroxide systems. Surf. Interface Anal. 41, 324–332. https://doi.org/10.1002/sia.3026.

Biesinger, M.C., Payne, B.P., Grosvenor, A.P., Lau, L.W.M., Gerson, A.R., Smart, R.S.C., 2011. Resolving surface chemical states in XPS analysis of first row transition metals, oxides and hydroxides: Cr, Mn, Fe. Co and Ni. Appl Surf Sci 257, 2717–2730. https://doi.org/10.1016/j.apsusc.2010.10.051.

Calvão F, Mcdonald CEA, Bolay M. Cobalt mining and the corporate outsourcing of responsibility in the Democratic Republic of Congo. Extractive Industries and Society 2021;8. DOI: 10.1016/j.exis.2021.02.004.

Chernysheva, D., Vlaic, C., Leontyev, I., Pudova, L., Ivanov, S., Avramenko, M., et al., 2018. Synthesis of Co_3O_4/CoOOH via electrochemical dispersion using a pulse alternating current method for lithium-ion batteries and supercapacitors. Solid State Sci 86, 53–59. https://doi.org/10.1016/j.solidstatesciences.2018.10.005.

EU Commission. Study on the review of the list of critical raw materials. 2017.

Crundwell, F.K., Moats, M.S., Ramachandran, V., Robinson, T.G., Davenport, W.G., 2011. Recycling of nickel, cobalt and platinum-group metals. Extractive metallurgy of nickel. Cobalt and Platinum Group Metals, Elsevier 537–549. https://doi.org/10.1016/b978-0-08-096809-4.10038-3.

Crundwell, F.K., Moats, M.S., Ramachandran, V., Robinson, T.G., Davenport, W.G., 2011. Cobalt – occurrence, production, use and Price. Extractive metallurgy of nickel. Cobalt and Platinum Group Metals, Elsevier 357–363. https://doi.org/10.1016/b978-0-08-096809-4.10028-0.

Das, D., Das, K., 2010. Cobalt hydroxide film on pt as co-catalyst for oxidation of polyhydric alcohols in alkaline medium. Mater Chem Phys 123, 719–722. https://doi.org/10.1016/j.matchemphys.2010.05.044.

Dehaine, Q., Tijsseling, L.T., Glass, H.J., Törmänen, T., Butcher, A.R., 2021. Geometallurgy of cobalt ores: a review. Miner Eng 160. https://doi.org/10.1016/j.mineng.2020.106656.

Faris, N., Fischmann, A.J., Assmann, S., Jones, L.A., Tardio, J., Madapusi, S., et al., 2021. A study into the behaviour of nickel, cobalt and metal impurities during partial neutralisation of synthetic nickel laterite pressure leach solutions and pulps. Hydrometall. 202 https://doi.org/10.1016/j.hydromet.2021.105604.

Giebner, F., Kaden, L., Wiche, O., Tischler, J., Schopf, S., Schlömann, M., 2019. Bioleaching of cobalt from an arsenidic ore. Miner Eng 131, 73–78. https://doi.org/10.1016/j.mineng.2018.10.020.

Godoy León, M.F., Dewulf, J., 2020. Data quality assessment framework for critical raw materials. the case of cobalt. Resour Conserv Recycl 157. https://doi.org/10.1016/j.resconrec.2019.104564.

Grujicic, D., Pesic, B., 2005. Iron nucleation mechanisms on vitreous carbon during electrodeposition from sulfate and chloride solutions. Electrochim Acta 50, 4405–4418. https://doi.org/10.1016/j.electacta.2005.02.013.

Gulley, A.L., 2022. One hundred years of cobalt production in the Democratic Republic of the Congo. Resour. Policy 79. https://doi.org/10.1016/j.resourpol.2022.103007.

Hägg M-B. Membrane purification of Cl_2 gas II. Permeabilities as function of temperature for Cl_2, O_2, N_2, H_2 and HCl in perfluorinated, glass and carbon molecular sieve membranes. vol. 177. 2000.

Harvey, R., Hannah, R., Vaughan, J., 2011. Selective precipitation of mixed nickel-cobalt hydroxide. Hydrometall. 105, 222–228. https://doi.org/10.1016/j.hydromet.2010.10.003.

Heli, H., Yadegari, H., 2010. Nanoflakes of the cobaltous oxide, CoO: synthesis and characterization. Electrochim Acta 55, 2139–2148. https://doi.org/10.1016/j.electacta.2009.11.047.

Ichlas, Z.T., Mubarok, M.Z., Magnalita, A., Vaughan, J., Sugiarto, A.T., 2020. Processing mixed nickel–cobalt hydroxide precipitate by sulfuric acid leaching followed by selective oxidative precipitation of cobalt and manganese. Hydrometall. 191 https://doi.org/10.1016/j.hydromet.2019.105185.

IEA The role of critical minerals in clean energy transitions 2021 Paris.

Jantunen, N, Virolainen, S, Sainio, T, 2022. Direct production of Ni–Co–Mn mixtures for cathode precursors from cobalt-rich lithium-ion battery leachates by solvent extraction. Metals (Basel) 12. https://doi.org/10.3390/met12091445.

Jung, H., Jun, Y.S., 2016. Ionic strength-controlled Mn (hydr)oxide nanoparticle nucleation on quartz: effect of aqueous $Mn(OH)_2$. Environ Sci Technol 50, 105–113. https://doi.org/10.1021/acs.est.5b02819.

N.D. Ivanova E.I. Boldyrev S. Ivanov, Makeeva IS. Electrochemical synthesis of black cobalt Russ. J. Appl. Chem. 76 2003 1631 1634.

Karami H, Chidar E. Pulsed Current Electrochemical Synthesis of Co_3O_4 Nanostructures. vol. 10. 2015.

A.A. Kasach D.S. Kharitonov I.V. Makarova A. Wrzesińska I.M. Zharskii I.I. Kurilo Effect of thiourea on electrocrystallization of Cu–Sn alloys from sulphate electrolytes Surf Coat Technol 399 2020 10.1016/j.surfcoat.2020.126137.

Kelpšaite, I., Baltrušaitis, J., Valatka, E., 2011. Electrochemical deposition of porous cobalt oxide films on AISI 304 type steel. Medziagotyra 17, 236–243. https://doi.org/10.5755/j01.ms.17.3.586.

Koga, N., Kimizu, T., Sakamoto, M., Furukawa, Y., 2009. Temperature effect on Cobalt (II)-chloride complex equilibrium in aqueous solution. Chem. Educ. 14, 52213–52218. https://doi.org/10.1333/s00897092213a.

Kouidri, N., Rahmane, S., Allag, A., 2019. Substrate temperature-dependent properties of sprayed cobalt oxide thin films. J. Mater. Sci. Mater. Electron. 30, 1153–1160. https://doi.org/10.1007/s10854-018-0384-3.

Kudielka, A., Bette, S., Dinnebier, R.E., Abeykoon, M., Pietzonka, C., Harbrecht, B., 2017. Variability of composition and structural disorder of nanocrystalline CoOOH materials. J Mater Chem C Mater 5, 2899–2909. https://doi.org/10.1039/c6tc04626f.

Li, H., Sun, C., Zhao, Y., Xu, X., Yu, H., 2018. Facile synthesis of recyclable Co_3O_4/Co$(OH)_2$/RGO ternary heterostructures with synergistic effect for photocatalysis. J. Nanopart. Res. 20 https://doi.org/10.1007/s11051-018-4359-3.

Lisnund, S., Blay, V., Muamkhunthod, P., Thunyanon, K., Pansalee, J., Monkrathok, J., et al., 2022. Electrodeposition of cobalt oxides on Carbon nanotubes for sensitive bromhexine sensing. Molecules 27. https://doi.org/10.3390/molecules27134078.

Liu, W., Li, X., Liu, C., Wang, M., Liu, L., 2023. Resilience assessment of the cobalt supply chain in China under the impact of electric vehicles and geopolitical supply risks. Resour. Policy 80. https://doi.org/10.1016/j.resourpol.2022.103183.

Liu, Z., Ma, R., Osada, M., Takada, K., Sasaki, T., 2005. Selective and controlled synthesis of α- and β-cobalt hydroxides in highly developed hexagonal platelets. J Am Chem Soc 127, 13869–13874. https://doi.org/10.1021/ja0523338.

Liu, G., Zhang, Y., Ni, Z., Huang, R., 2016. Corrosion behavior of steel submitted to chloride and sulphate ions in simulated concrete pore solution. Constr Build Mater 115, 1–5. https://doi.org/10.1016/j.conbuildmat.2016.03.213.

Makarova, I., Ryl, J., Sun, Z., Kurilo, I., Górnicka, K., Laatikainen, M., et al., 2020. One-step recovery of REE oxalates in electro-leaching of spent NdFeB magnets. Sep Purif Technol 251. https://doi.org/10.1016/j.seppur.2020.117362.

Metz, R., Morel, J., Delalu, H., Ananthakumar, S., Hassanzadeh, M., 2010. Full transition from metal to ceramic by direct oxidation of metallic cobalt powder. Ceram Int 36, 855–862. https://doi.org/10.1016/j.ceramint.2009.10.010.

Moysiadou, A., Lee, S., Hsu, C.S., Chen, H.M., Hu, X., 2020. Mechanism of oxygen evolution catalyzed by cobalt oxyhydroxide: cobalt superoxide species as a key intermediate and dioxygen release as a rate-determining step. J Am Chem Soc 142, 11901–11914. https://doi.org/10.1021/jacs.0c04867.

Pontinha, M., Faty, S., Walls, M.G., Ferreira, M.G.S., Da Cunha Belo, M., 2006. Electronic structure of anodic oxide films formed on cobalt by cyclic voltammetry. Corros Sci 48, 2971–2986. https://doi.org/10.1016/j.corsci.2005.10.007.

Rahimpour Golroudbary, S., Farfan, J., Lohrmann, A., Kraslawski, A., 2022. Environmental benefits of circular economy approach to use of cobalt. Glob. Environ. Chang. 76 https://doi.org/10.1016/j.gloenvcha.2022.102568.

Scheck, J., Wu, B., Drechsler, M., Rosenberg, R., Van Driessche, A.E.S., Stawski, T.M., et al., 2016. The molecular mechanism of iron(III) oxide nucleation. J. Phys. Chem. Lett. 7, 3123–3130. https://doi.org/10.1021/acs.jpclett.6b01237.

Spasojević, M., Ribić-Zelenović, L., Spasojević, P., 2012. Microstructure of new composite electrocatalyst and its anodic behavior for chlorine and oxygen evolution. Ceram Int 38, 5827–5833. https://doi.org/10.1016/j.ceramint.2012.04.032.

Surendranath, Y., Lutterman, D.A., Liu, Y., Nocera, D.G., 2012. Nucleation, growth, and repair of a cobalt-based oxygen evolving catalyst. J Am Chem Soc 134, 6326–6336. https://doi.org/10.1021/ja3000084.

Tan, W., He, H., Gao, Y., Peng, Y., Dai, X., 2021. Nucleation and growth mechanisms of an electrodeposited Ni–Se–Cu coating on nickel foam. J Colloid Interface Sci 600, 492–502. https://doi.org/10.1016/j.jcis.2021.05.002.

Tombácz, E., 2009. pH-dependent surface charging of metal oxides. Period. Polytech., Chem. Eng. 53, 77–86. https://doi.org/10.3311/pp.ch.2009-2.08.

Torjus, Å., 2008. Electrowinning of cobalt from chloride solutions: anodic deposition of cobalt oxide on DSA. Norwegian University of Science and Technology.

Urgunde, A.B., Kamboj, V., Kannattil, H.P., Gupta, R., 2019. Layer-by-layer coating of cobalt-based ink for Large-scale fabrication of OER electrocatalyst. Energ. Technol. 7 https://doi.org/10.1002/ente.201900603.

Välikangas, J., Laine, P., Hietaniemi, M., Hu, T., Tynjälä, P., Lassi, U., 2020. Precipitation and calcination of high-capacity $LiNiO_2$ cathode material for lithium-ion batteries. Applied Sciences (switzerland) 10, 1–11. https://doi.org/10.3390/app10248988.

Vittal, R., Ho, K.C., 2015. Cobalt oxide electrodes-problem and a solution through a novel approach using cetyltrimethylammonium bromide (CTAB). Catal Rev Sci Eng 57, 145–191. https://doi.org/10.1080/01614940.2015.1035192.

Vos, J.G., Liu, Z., Speck, F.D., Perini, N., Fu, W., Cherevko, S., et al., 2019. Selectivity trends between oxygen evolution and chlorine evolution on iridium-based double perovskites in acidic media. ACS Catal 9, 8561–8574. https://doi.org/10.1021/acscatal.9b01159.

Yu, Y., Wang, H., Zhang, H., Tan, Y., Wang, Y., Song, K., et al., 2020. Blanket-like Co $(OH)_2$/CoOOH/Co_3O_4/$Cu(OH)_2$ composites on cu foam for hybrid supercapacitor. Electrochim Acta 334. https://doi.org/10.1016/j.electacta.2019.135559.

Yuan L, Yang H, Ning P, Wen J, Sun Z, Cao H. Green separation and recovery of cobalt and nickel from sulphuric acid achieved by complexation-assisted solvent extraction. Sep Purif Technol 2022;286. DOI: 10.1016/j.seppur.2021.120343.

Zhang N, Fan Y, Fan H, Shao H, Wang J, Zhang J, et al. Cross-linked Co_3O_4 nanowalls synthesized by electrochemical oxidation of metallic cobalt layer for oxygen evolution. ECS Electrochemistry Letters 2012;1. DOI: 10.1149/2.013202eel.

Zheng C, Jiang K, Cao Z, Wang H, Liu S, Waters KE, et al. Pressure leaching behaviors of copper-cobalt sulfide concentrate from Congo. Sep Purif Technol 2023;309. DOI: 10.1016/j.seppur.2022.123010.

Zhou, X., Wang, Y., Liang, Z., Jin, H., 2018. Electrochemical deposition and nucleation/growth mechanism of Ni-Co-Y_2O_3 multiple coatings. Materials 11. https://doi.org/10.3390/ma11071124.

Zhou, W.J., Xu, M.W., Zhao, D.D., Xu, C.L., Li, H.L., 2009. Electrodeposition and characterization of ordered mesoporous cobalt hydroxide films on different substrates for supercapacitors. Microporous Mesoporous Mater. 117, 55–60. https://doi.org/10.1016/j.micromeso.2008.06.004.